

The sizes of galaxy halos in galaxy cluster Abell 1689

A. Halkola and S. Seitz

Universitäts-Sternwarte München, Scheinerstraße 1, D-81679 München, Germany

halkola@usm.uni-muenchen.de

and

M. Pannella

Max-Planck-Institut für extraterrestrische Physik, Giessenbachstraße, Postfach 1312, D-85741 Garching, Germany

ABSTRACT

The multiple images observed in galaxy cluster Abell 1689 provide strong constraints not only on the mass distribution of the cluster but also on the ensemble properties of the cluster galaxies. Using parametric strong lensing models for the cluster, and by assuming well motivated scaling laws between the truncation radius s and the velocity dispersion σ of a cluster galaxy we are able to derive sizes of the dark matter halos of cluster galaxies.

For the scaling law expected for galaxies in the cluster environment ($s \propto \sigma$), we obtain $s = 64_{-14}^{+15} \times (\sigma / 220 \text{ km/s})$ kpc. For the scaling law used for galaxies in the field with $s \propto \sigma^2$ we find $s = 66_{-16}^{+18} \times (\sigma / 220 \text{ km/s})^2$ kpc. Compared to halos of field galaxies, the cluster galaxy halos in Abell 1689 are strongly truncated.

Subject headings: gravitational lensing – cosmology:dark matter – galaxies:clusters:individual:Abell 1689

1. Introduction

Although galaxies are the units of objects seen on cosmological distances, very little is known observationally about the extent of dark matter halos surrounding the galaxies beyond the light emitted by the gas and stars in them. Based on numerical simulations these dark matter halos are expected to extend out to several hundred kpc (e.g. Tormen et al. 1998). Rotation curves of spiral galaxies and the line of sight velocity dispersions of the stars in elliptical galaxies can be measured only out to some tens of kiloparsecs (see e.g. Sofue & Rubin 2001; Bender et al. 1994 and references therein). The results from these two methods indicate that the masses of galaxies continue to grow roughly linearly with the radius, i.e. the matter in galaxies is closely isothermal. The radial velocities of satellites of galaxies can also be used to estimate the masses of their host galaxies (e.g. Hartwick & Sargent 1978; Zaritsky et al.

1989; Prada et al. 2003). This has recently been done for the Milky Way by Battaglia et al. (2005) who were able to measure the radial velocity dispersion profile of the Galaxy out to 120 kpc. The method works only for field galaxies since it is sensitive to other nearby massive galaxies and hence the galaxies studied need to be isolated (Brainerd 2004).

Gravitational lensing is an ideal tool to measure the extents of dark matter halos around galaxies since no optical tracers within the halo are needed. Instead, the halo mass can be inferred from the gravitational lensing of background sources.

Weak lensing can be used to study galactic dark matter halos statistically. The field started from the pioneering work of Tyson et al. (1984), and galaxy-galaxy lensing has now been successfully used both in the field (Brainerd et al. 1996; dell’Antonio & Tyson 1996; Hudson et al. 1998;

Fischer et al. 2000; Smith et al. 2001; Wilson et al. 2001; McKay et al. 2001; Hoekstra 2003; Hoekstra et al. 2004) and in clusters (Natarajan et al. 1998; Geiger & Schneider 1999; Natarajan et al. 2002; Gavazzi et al. 2004; Limousin et al. 2006) to measure the masses and extents of galaxy halos. The signal is very weak for individual galaxies and needs to be collected from many galaxies, possibly adopting various scaling laws to compare measurements from lensing galaxies with different luminosities. The different works generally find a tangential shear γ that decreases like $\gamma \propto 1/\theta$ with the radius θ , i.e. the halos stay roughly isothermal beyond the luminous component. In the field the signal from galaxies has been measured out to ~ 200 kpc (e.g. Wilson et al. 2001; Hoekstra et al. 2004).

The galaxy truncation in clusters has been studied both theoretically and observationally in Natarajan & Kneib (1997); Natarajan et al. (1998); Geiger & Schneider (1998, 1999); Natarajan et al. (2002); Gavazzi et al. (2004); Limousin et al. (2005, 2006). Strong truncation of galaxies is found in Natarajan et al. (1998), Natarajan et al. (2002) and Limousin et al. (2006) when compared to galaxies in the field (truncation radii s^* of L^* galaxies span 17-55 kpc in the 6 clusters vs. $s^*=264\pm42$ kpc/ h_{70} in the field, Hoekstra et al. 2004). There is a general agreement that the halos of galaxies in dense environments are truncated relative to those in the field although the uncertainties are still large and the sample of clusters used is inhomogeneous. The inherently statistical nature of the methods and the need to assume certain scaling laws further complicate the case. The method used in Natarajan et al. (1998, 2002) also requires that the parameters of the smooth cluster component are known accurately (Natarajan & Kneib 1997). This is achieved by incorporating also strong lensing constraints in the clusters enabling Natarajan et al. to accurately model the cluster profile.

The typical radius of an Einstein ring of a galaxy is at most a few arcseconds and so in the strong lensing regime it is not possible to probe the extent of dark matter halos beyond a few arcseconds directly. This makes strong lensing unfeasible to study the dark halos of individual galaxies beyond a few arcseconds in the field. In clusters of galaxies however the combined potentials of the

smooth dark matter halo of the cluster as a whole and those of the individual galaxy halos are responsible for the lensing of background sources. This enables us to statistically probe galaxy halos in dense environments using strong gravitational lensing. Since lensing constrains only the total potential of the cluster it is important to have a large number of multiple images with a large radial spread over the cluster in order to investigate the different mass components separately. Abell 1689 is ideally suited for this task with the large number of identified multiple images of many different background sources and well defined strong lensing models (Broadhurst et al. 2005; Diego et al. 2005; Zekser et al. 2006; Halkola et al. 2006). In this paper we use the strong lensing models developed in Halkola et al. (2006) to study the truncation of cluster galaxy dark matter halos in A1689. We demonstrate that the models are indeed sensitive to the total mass contained in the cluster galaxies and derive sizes for the galaxies in the cluster. This is the first time the sizes of galaxy halos have been measured in dense cluster environments with strong lensing only.

In section 2 we give a brief summary of the models used in Halkola et al. (2006) in particular the modeling of the galaxy component of the cluster, in section 3 we outline the methodology used to study the truncation of the cluster galaxies. The results are presented in section 4 and in section 5 we perform several checks to demonstrate that the results obtained are robust and reasonable. In section 6 we compare the results with earlier published studies of galaxy halo truncation before concluding in section 7.

The cosmology used throughout this paper is $\Omega_m=0.30$, $\Omega_\Lambda=0.70$ and $H_0=70$ km/s/Mpc.

2. Strong Gravitational Lensing Model for A1689

The strong lensing models in this work are based on the parametric models used in Halkola et al. (2006) to study the mass profile of A1689 in detail. Here we give a short summary of the strong lensing modeling but refer the reader to Halkola et al. (2006) for the details.

The multiple images in Halkola et al. (2006)

were in most part those identified in Broadhurst et al. (2005). In total a 107 multiple images in 31 multiple image systems and 1 arc were used. In 5 cases at least one of the images in a system had also a spectroscopic redshift and the redshifts were kept fixed for these systems. The redshifts of another 26 multiple image systems were estimated using photometric redshifts. In these cases the redshift of an image system was allowed to find its best redshift within the estimated photometric redshift errors. The arc was too faint for good photometry and its redshift is left unconstrained.

The mass in the cluster is assumed to be in two smooth DM halos that are described by either non-singular isothermal ellipsoids (NSIE) or elliptical Navarro-Frenk-White profiles (ENFW). The small scale mass structures associated with the galaxies are modeled with BBS profiles (Brainerd et al. 1996). The BBS profile is a singular isothermal sphere with a truncation radius s . In the central regions ($r < s$) the density profile is isothermal ($\rho \propto r^{-2}$) but there is a truncation of the halo at radius s after which the density falls sharply with $\rho \propto r^{-4}$.

The velocity dispersions of the galaxies are estimated using the Fundamental Plane (FP). The FP ties kinematic (velocity dispersion), photometric (effective surface brightness) and morphological (half light radius) galaxy properties together (Dressler et al. 1987; Djorgovski & Davis 1987; Bender et al. 1992). Measuring morphological and photometric properties of the galaxies allows us to estimate the galaxy kinematics. We assume that the central velocity dispersions of galaxies, as derived from the FP, are equal to the halo velocity dispersions, and that the masses in disks can be neglected. For some fainter galaxies we have also used the Faber-Jackson relation (Faber & Jackson 1976, here after FJ relation) that relates the absolute magnitude of a galaxy to its velocity dispersion. The FJ relation has a large intrinsic scatter and the velocity dispersion obtained using FJ have a larger uncertainty than the ones obtained with the FP.

The truncation radii of the galaxies are assumed to follow a scaling law of the form $s_{gal} = s^0 \times (\sigma_{gal}/\sigma^0)^\alpha$. In this paper we discuss the same scaling laws as in Halkola et al. (2006), namely $\alpha = 1$ and $\alpha = 2$. $\alpha=1$ corresponds to tidal truncation of halos in dense cluster en-

vironment (Merritt 1983) whereas galaxies with $\alpha=2$ have a constant mass-to-light ratio and is usually assumed in weak lensing analyses (e.g. Brainerd et al. 1996; Natarajan et al. 1998; Hoekstra et al. 2004). In this paper we explore further the radial extent of the galaxy halos for the scaling laws used in Halkola et al. (2006).

A1689 is an excellent candidate for this work since the large number of multiple images ensures not only that the global mass profile can be constrained very accurately but also the relative contributions of the smooth DM and galaxies can be determined as will be shown later.

3. Methodology

In this paper take advantage of the unique opportunity presented in A1689 to use strong lensing and the significant contribution of the cluster galaxies on the positions of the impressive number of multiple images observed in the cluster. The effect is only observable in the total fit quality and is hence statistical in nature in that extension of individual galaxies cannot be determined.

Unlike the usual galaxy-galaxy lensing in which foreground galaxies weakly distort the shapes of background galaxies this method relies on the changes induced by galaxies on the *positions* of multiply imaged background galaxies. This strong galaxy-galaxy lensing is only applicable in the strong lensing regime where multiple images are observed over a large range of cluster centric radii so that they pose strong constraints both on the total cluster potential and also on the galaxies.

In this section we outline the method used to measure the extents of galaxy halos. The strong lensing models are constrained by the observed multiple images. The positions of the images can be measured to an accuracy of better than 1 pixel or 0.05" on the images from the Advanced Camera for Surveys. The only other measurables are the redshifts of the cluster and the multiple images. The redshift of the cluster is well established from spectroscopic surveys (Teague et al. 1990; Balogh et al. 2002; Duc et al. 2002) and the overall mass scale of the cluster is fixed by the 5 spectroscopic redshifts of multiple image systems. The major uncertainty in the models is the inclusion of the cluster galaxies. In the following we describe the Monte-Carlo simulations used to find

the normalization of the scaling law, s^0 , and how these simulations can also be used to estimate the error in s^0 due to the uncertainties in the observables.

3.1. Monte-Carlo Simulations

A Monte-Carlo run consists of reassigning a new velocity dispersion, σ_{MC} , to each cluster galaxy based on the value σ_{gal} and estimated error determined using the FP or the FJ relation. The new σ_{MC} of a galaxy was drawn from a Gaussian distribution centered on σ_{gal} with a width corresponding to the estimated error. The multiple image positions were similarly varied with assumed error of 1 pixel. In this way we have constructed a simulated galaxy that has properties similar to the one observed within our estimates of the errors.

This cluster can now be analyzed in the same way as the 'original' cluster. This means that we find the optimal parameters for the two smooth DM halos (positions, ellipticities, position angles and the two free parameters of the halos: velocity dispersion and core radius for the NSIE profile and concentration and virial radius for the ENFW profile) and redshifts for the image systems with photometric redshifts.

The simulated clusters used in this work are the same that were used in Halkola et al. (2006) to derive errors for the total mass profile and the parameters of smooth DM halo.

In this work we concentrate on the normalization of the truncation radius s^0 for two scaling laws, $\alpha = 1$ and $\alpha = 2$, which was not done in Halkola et al. (2006). This means that in addition to optimizing the above mentioned parameters we also find the optimal value of s^0 for each simulated cluster. This is explained below.

3.2. Determining s^0 for a Monte-Carlo Run

The optimal s^0 for each Monte-Carlo run was taken as the one with the minimum $\langle \chi^2 \rangle^{1/2}$ when s^0 was progressively increased from 20 kpc to 200 kpc. The parameter optimization was performed by a source plane minimization for computational reasons. In all subsequent analysis we have used an image plane χ^2 defined as the sum of the squared distances between the observed images and ones predicted by our models. $\langle \chi^2 \rangle^{1/2}$

is hence the rms distance between the observed images and the corresponding model image positions.

We use the shapes of these $\langle \chi^2 \rangle^{1/2}$ vs. s^0 curves to convince the reader that there is clear signal and that s^0 can be constrained in clusters using strong lensing once sufficiently many multiple images can be used to constrain the models.

3.3. Determining s^0 for the Cluster

The shape and spread of the $\langle \chi^2 \rangle^{1/2}$ vs. s^0 curves could in principle also be used to derive confidence limits on s^0 . This, however, would require us to perform more simulations to derive appropriate $\Delta\chi^2$ levels for the confidence limits. The $\langle \chi^2 \rangle^{1/2}$ vs. s^0 curves do however demonstrate that there is a strong and clean signal that can be used to derive s^0 and the errors for a given scaling law.

The best fitting s^0 and the errors for the cluster are derived from the distribution of the s^0 values obtained in the Monte-Carlo runs instead.

4. Results

For the scaling law we need to choose a reference σ^0 . The derived s^0 is then the truncation radius of a galaxy with a velocity dispersion equal to this σ . The truncation radii of galaxies with different σ s can then be obtained using the appropriate scaling law. In this work we simply assume a fiducial value of $\sigma^0 = 220$ km/s. To compare the s^0 obtained in this work with literature one should scale our s^0 by $(\sigma_{lit}^0 / 220 \text{ km/s})^\alpha$.

In creating the simulated clusters the velocity dispersions for the galaxies are drawn from a Gaussian distribution and hence we do not expect to see significant differences in the shapes of the individual $\langle \chi^2 \rangle^{1/2}$ vs. s^0 curves between the different Monte-Carlo runs that would arise from a systematic change in the galaxy component. The curves do vary in their absolute $\langle \chi^2 \rangle^{1/2}$ level however. For this reason we have normalized the individual curves to their respective median $\langle \chi^2 \rangle^{1/2}$ in order to bring all the curves to a similar $\langle \chi^2 \rangle^{1/2}$ level. After this the curves have been renormalized to the level of the mean median $\langle \chi^2 \rangle^{1/2}$ of all the curves. The scaling of the individual curves is necessary in order to combine the information on

s^0 from the different curves.

In Fig. 1 the mean curves for 1000 simulated clusters for each of the smooth DM profiles used are shown. NSIE is shown as a dotted line and squares, ENFW as a dashed line and triangles. The left panel shows the curves for $\alpha = 1$ ($s \propto \sigma$) and the right for $\alpha = 2$ ($s \propto \sigma^2$). Combining the two smooth DM profiles yields the solid line and points shown as circles. The points show the 2-sigma clipped mean for each s^0 . The error bars show the dispersions of the final clipped points for a given s^0 .

The smaller scatter in the points for NSIE models is an indication that the renormalized curves are very similar while the considerable scatter for the ENFW models shows that the curves differ not only in the absolute χ^2 level but also in their shape. The combined curve has been calculated from the NSIE and ENFW curves and not from the curves of each individual Monte-Carlo run for the two models. ENFW smooth DM profiles generally favor slightly larger values for s^0 than the NSIE models ($\Delta s^0 \sim 10$ kpc).

The $\langle \chi^2 \rangle^{1/2}$ vs. s^0 curves are flatter at large (>50 kpc) s^0 than at smaller s^0 , this is especially apparent for the cases where the smooth DM is described by an NSIE profile. A possible reason for the shallower slope on the logarithmic horizontal scale (linear in fractional change in mass) in Fig. 1 is that the larger extent of the halos, and hence a smoother combined mass profile of the galaxies, makes it easier for the smooth DM component to compensate for the change in the mass in the galaxies. In the small s^0 regime the galaxies have significant local contribution to the image positions which cannot be easily compensated by the smooth DM component.

The curves for the two scaling laws are very similar and we are not able to differentiate between them in terms of quality of fit. This is also seen in weak lensing determinations of the extensions of the dark matter halos of galaxies (Limousin 2006, private communication). A possible explanation is that instead of measuring the extension directly we are in fact measuring the mass of the galaxies. This then creates a degeneracy between the two parameters in the scaling law, namely α and s^0 .

For a different value of α the same total mass in the galaxies can be obtained by appropriately adjusting s^0 .

We would like to stress at this point that the two panels in Fig. 1 are only shown to illustrate that the s^0 is indeed constrained and to provide an idea how the fit quality changes when s^0 deviates from the best fit s^0 . The $\langle \chi^2 \rangle^{1/2}$ vs. s^0 curves are not used to derive the s^0 of the cluster nor the errors. The estimation of s^0 and errors is done using the histograms of the S^0 s obtained using the Monte-Carlo simulations shown in Fig. 2 and explained below.

We finally use the best fitting s^0 of each Monte-Carlo run to derive s^0 for A1689 and estimate the errors. In Fig. 2 we show the histograms of s^0 values at which each simulated cluster attains its minimum $\langle \chi^2 \rangle^{1/2}$, i.e. the best fitting s^0 for a given Monte-Carlo run.

As is expected the histograms peak nicely at the positions where the mean curves in Fig. 1 also have their minima. The strong clustering of the histograms between $s^0 = 40$ kpc and $s^0 = 90$ kpc with only a few outliers demonstrates that s^0 is well constrained. The flatter $\langle \chi^2 \rangle^{1/2}$ vs. s^0 curves at $s^0 > 50$ kpc for the NSIE models lead to less well defined minima and correspondingly wider distribution of s^0 at large s^0 in the histograms.

The best fit values of s^0 for the different descriptions of the smooth DM component of the cluster are shown in Table 1. The values given are the geometric means of the best fit s^0 of all the simulated clusters. We have used the geometric mean to estimate the truncation radius since this corresponds to fractional change in mass and the $\langle \chi^2 \rangle^{1/2}$ vs. s^0 curves in Fig. 1 are relatively symmetric in $\log(s^0)$ (although not exactly as discussed earlier). We also give in Table 1 the estimated 1- and 2- σ errors of s^0 . The errors have been derived from the distribution of the best fit s^0 of the simulated clusters shown in Fig. 2. For this the histograms were interpreted as probability distributions of s^0 and 1- and 2- σ confidence intervals were estimated by the regions around the mean that contain 68.3 per cent and 95.4 per cent of the best fit s^0 values from the simulation for the 1- and 2- σ errors respectively. The asymmetry of the distribution becomes evident at higher

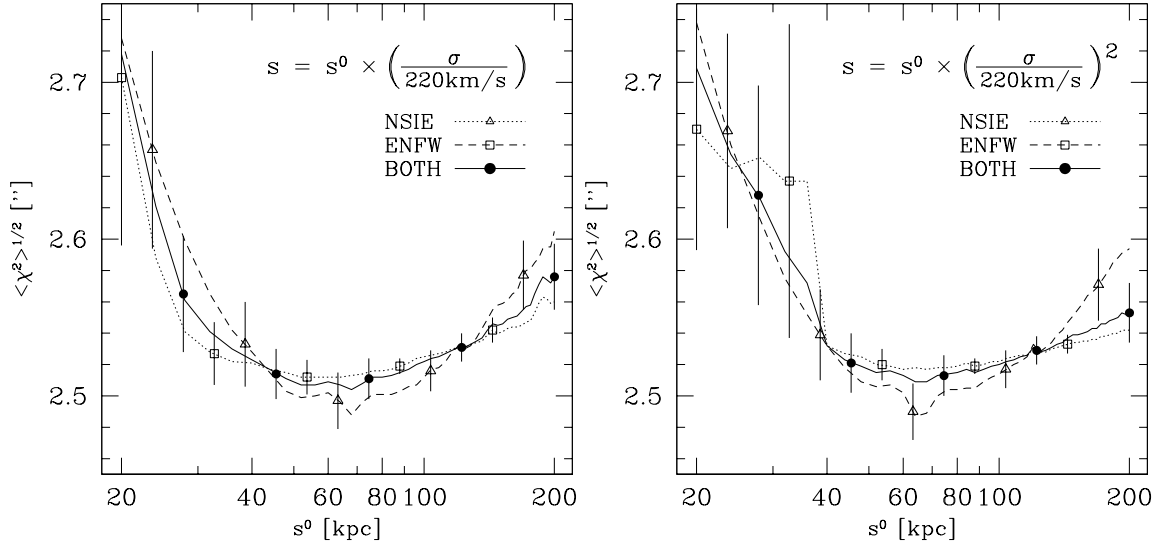


Fig. 1.— The mean $\langle \chi^2 \rangle^{1/2}$ vs. s^0 curve for 1000 simulated clusters for the smooth DM described by both NSIE (dotted line, squares) and ENFW (dashed line, triangles), and the combined data from the two smooth profiles (solid line, circles). The left panels are calculated for the scaling of the truncation radius with $s \propto \sigma$ and the right panels for $s \propto \sigma^2$. The points show the 2-sigma clipped mean for each s^0 , and the error bars show the final sigma of the clipped points. Before clipping, the individual curves were normalized to their median $\langle \chi^2 \rangle^{1/2}$ in order to bring all the curves to a similar $\langle \chi^2 \rangle^{1/2}$ level for comparison. The median curve has been brought back to the level of the mean median $\langle \chi^2 \rangle^{1/2}$. The combined curve has been calculated from the NSIE and ENFW curves and not from the individual curves for the two models. The minimum $\langle \chi^2 \rangle^{1/2}$ is obtained at ~ 60 - 70 kpc.

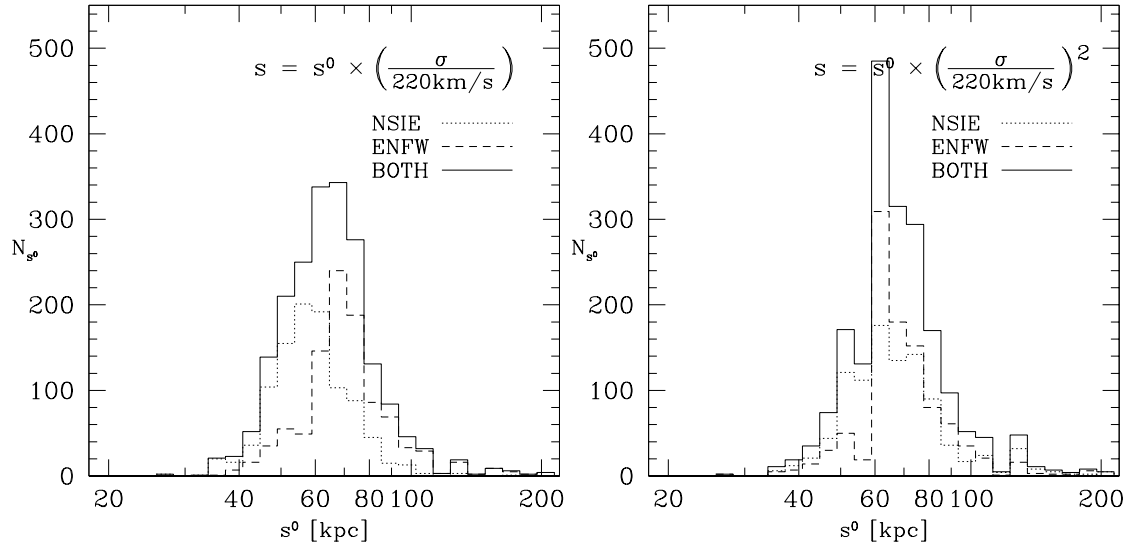


Fig. 2.— The histograms of the s^0 values at which each simulated cluster attains its minimum. The line types used are as above. As is expected, the histograms peak nicely at the positions where the mean curves on the top row also have their minima. The strong clustering of the histogram between $s^0 = 40$ kpc and $s^0 = 90$ kpc with only a few outliers demonstrates that s^0 is strongly constrained. The best fit s^0 and its error has been derived from these histograms.

confidence limits as can be seen in the 2σ errors.

For the scaling law expected theoretically for galaxies in clusters (Merritt 1983), $s = s^0 \times (\sigma / \sigma^0)$, we find $s^0 = 64^{+67}_{-28}$ kpc, where the errors given are 2σ errors. For the scaling law used for galaxies in the field ($s = s^0 \times (\sigma / \sigma^0)^2$), we find $s^0 = 66^{+72}_{-26}$ kpc, the errors are again 2σ errors.

5. Checks on the Robustness of the Results

We have performed the following checks to confirm that the results presented above are reasonable and robust.

5.1. σ^0 , s^0 , α and the Total Mass in Cluster Galaxies

The total mass of a galaxy with a BBS profile can be easily written in terms of its truncation radius s and velocity dispersion σ as is shown in Brainerd et al. (1996). The total mass of the cluster galaxies in A1689 with a scaling law for the truncation of the halos of the form $s = s^0 \times (\sigma / \sigma^0)^\alpha$ can be written simply as,

$$M_{tot} = 7.3 \times 10^5 \left(\frac{s^0}{\text{kpc}} \right) \sum_i \left(\frac{\sigma_i}{\text{km/s}} \right)^2 \left(\frac{\sigma_i}{\sigma^0} \right)^\alpha M_\odot, \quad (1)$$

where s^0 is the normalization of the scaling law, σ^0 a reference velocity dispersion and σ_i is the velocity dispersion of galaxy i .

In our study we have taken $\sigma^0 = 220$ km/s. Note that this σ^0 is only a fiducial value and is not related to the L^* of the galaxies in the cluster. With this σ^0 and our set of galaxies in the cluster, the galaxies have the same total mass with the two scaling laws ($\alpha=1$ and $\alpha=2$) if $s_{\alpha=2}^0 = 0.93 \times s_{\alpha=1}^0$. Note that this relation between $s_{\alpha=1}^0$ and $s_{\alpha=2}^0$ is the same for all $s_{\alpha=1}^0$ and $s_{\alpha=2}^0$.

The fact that the normalizations s^0 obtained for the two scaling laws are very similar ($s_{\alpha=1}^0 = 64^{+15}_{-14}$ kpc and $s_{\alpha=2}^0 = 66^{+18}_{-16}$ kpc) for $\sigma^0 = 220$ km/s provides strong support for the results and our analysis.

5.2. Sensitivity of Cluster Lensing to Extensions of Galaxy Halos

To demonstrate that we are indeed able to measure the extension of galaxy DM halos with strong lensing we have created clusters with an s^0 in the range [20,80] kpc. For each of these clusters we have created a mock set of multiple images that are exactly reproduced by the cluster. The mock multiple image set is based on the observed multiple images so that the cluster setup is as close to reality as possible. These clusters with known galaxy truncation laws are then analyzed in the same way as is done for A1689.

We find that we are able to recover the input s^0 within a few kpc in all cases. Additionally, both the change in the fit quality ($\Delta \langle \chi^2 \rangle^{1/2} \sim 0.2''$) of these new simulated clusters and the distribution of the best fit s^0 is similar to what is observed and shown in Figures 1 and 2.

5.3. Effect of the Choice of Multiple Image Systems

We have in addition checked the sensitivity of the results to our choice of multiple images. This was done by running another 100 Monte-Carlo runs with $\alpha=1$ and the smooth DM described by NSIE profiles. This time for each Monte-Carlo run we selected randomly 20 of the 32 image systems to use as constraints for the modeling. The multiple images with spectroscopic redshifts were always included since they are needed to fix the overall mass scale of the cluster. With fewer constraints we obtained essentially the same s^0 with larger spread in the distribution of s^0 from the different runs. The best fit s^0 obtained with 20 image systems is $s^0 = 59^{+27}_{-19}$ kpc compared to $s^0 = 58^{+12}_{-11}$ kpc with all the image systems, the errors are 1σ .

When only 20 multiple image systems were used the absolute $\langle \chi^2 \rangle^{1/2}$ stayed at the same level as with all the 32 image systems. This shows that the $\langle \chi^2 \rangle^{1/2}$ level is not driven by only a few image systems but all image systems contribute similarly to the $\langle \chi^2 \rangle^{1/2}$ level. The change in fit quality between best fit s^0 and extrema at $s^0 = 20$ kpc and $s^0 = 200$ kpc with fewer image systems is $\Delta \langle \chi^2 \rangle^{1/2} \sim 0.1''$ showing that also the individual s^0 are less well constrained with fewer image systems. That no change in s^0 is obtained

Table 1: Derived s^0 values and 1- and 2- σ errors for s^0 for the different descriptions of the smooth DM component of cluster. The truncation radius s of a galaxy depends on its velocity dispersion σ and the scaling laws adopted are of the form $s = s^0 \times (\sigma/\sigma^0)^\alpha$. The s^0 values given are the geometric means of the individual minima of the simulated clusters. The errors are derived from the distribution of the minima. We give both 1- and 2- σ errors since the asymmetries of the distributions become more apparent at higher confidence limits. The histograms of the minima for the different descriptions of smooth DM are shown in Fig. 2.

Smooth DM profile	α	s^0 (kpc)	1- σ errors (kpc)	2- σ errors (kpc)
NSIE	1	58	+12 / -11	+32 / -23
ENFW	1	69	+19 / -12	+88 / -30
NSIE & ENFW	1	64	+15 / -14	+67 / -28
NSIE	2	64	+18 / -15	+76 / -25
ENFW	2	66	+18 / -16	+70 / -26
NSIE & ENFW	2	66	+18 / -16	+72 / -26

demonstrates that our results for s^0 are robust.

6. Comparison with literature

The extensions of dark matter halos have been measured previously in cluster environment by Natarajan et al. (1998), Natarajan et al. (2002), Gavazzi et al. (2004), and Limousin et al. (2006).

Strong truncation of galaxies is found in Natarajan et al. (1998), Natarajan et al. (2002), and Limousin et al. (2006) when compared to galaxies in the field; the truncation radii of an L_* galaxy span the range 17-55 kpc for the 6 clusters studied in Natarajan et al. (2002). The halos in Limousin et al. (2006) are truncated more with a typical truncation radius below 20 kpc.

An important difference in the analysis of Natarajan et al. (1998, 2002) to that of Limousin et al. (2006) is that Natarajan et al. also include strong lensing features in the central parts of the clusters to further constrain the mass profile of the selected cluster sample and hence also constrain the galaxy halo parameters stronger. This helps to better define the shear contribution from the cluster galaxies and hence the truncation radius. Another major difference is that Limousin et al. (2006) work exclusively with ground based data where as Hubble Space Telescope data are used in Natarajan et al. (1998, 2002).

The large errors in the work of Gavazzi et al. are caused by the smoothing scale of $\theta_s = 220 \text{ kpc}/h_{70}$ employed in their analysis which restricts the

achievable resolution. Although they are not able to derive strong limits on the sizes of cluster galaxies, they do find that halos on the periphery of the cluster MS0302+17 are more strongly truncated than the halos on the central regions of the cluster providing thus further confirmation for the tidal stripping scenario.

For the range of σ^0 's for the clusters in Natarajan et al. (2002) our s^0 is in the range [32,66] kpc for $\alpha = 1$ and [16,72] kpc for $\alpha = 2$ (their s^0 span 17-55 kpc). In Fig. 3 we show a comparison between our results and those of Natarajan et al. (2002) and Limousin et al. (2006). For our points we also show the scaling of s^0 with σ^0 as dotted and dashed lines ($\alpha = 1$ and $\alpha = 2$ respectively). The lines can be used to convert the s^0 and errors to a σ^0 different from 220 km/s, making the comparison between other works easier. The solid line shows the $s-\sigma$ pairs for a galaxy with a total mass of $5 \times 10^{11} M_\odot$. The scatter of the points is large, though mostly consistent within the large error bars. There is some indication that the galaxy halos in A1689 are more extended than those in most of the other cluster studied.

Natarajan et al. (2002) compared their results for the density of the cluster at the core radius, $\rho(r_c)$, and the truncation radius of galaxies obtained in their analysis and found results in good agreement with Merritt (1983),

$$s^0 = 40 \frac{\sigma^0}{180 \text{km/s}} \left(\frac{\rho(r_c)}{3.95 \times 10^6 M_\odot \text{kpc}^{-3}} \right)^{-0.5} \text{kpc.} \quad (2)$$

Using the results for A1689 ($\sigma_{\text{cluster}} = 1450 \text{ km/s}$ and $r_c = 77 \text{ kpc}$, Halkola et al. 2006) we get an expected truncation radius of 54 kpc, a little smaller than the ~ 65 kpc obtained in this work. This (small) difference is in fact also expected since in our analysis we measure the truncation radii of the galaxies along the line of sight. Some of the galaxies will have large cluster-centric distances despite their small projected distances from the center. This supports the idea that the galaxy clusters are mainly truncated by the tidal field of the global potential as assumed by Merritt (1983) and also shown in numerical simulations by Moore et al. (1998); Ghigna et al. (2000).

When comparing the results from different works it should be noted that weak lensing works generally include all the galaxies from the center to the periphery of the cluster (although Gavazzi et al. 2004 do separate the galaxies in radius). This means that the results are averaged over the cluster galaxy population out to several Mpc (Limousin et al. 2006). With our strong lensing method we include galaxies only out to a projected cluster-centric radius of $r \sim 300$ kpc. The clusters also vary in their central densities complicating direct comparison between clusters. According to Limousin et al. (2006) their cluster sample (Abell clusters A1763, A1835, A2218, A383 and A2390) form a homogeneous set of clusters and hence the results for these clusters should be comparable.

Comparison to field galaxies is shown in Fig. 4. In the figure we show points from Brainerd et al. (1996), Fischer et al. (2000), Smith et al. (2001), Hoekstra (2003) and Hoekstra et al. (2004). Adopting $\sigma_{136}^0 = 136 \text{ km/s}$ used by Hoekstra et al. (2004) we obtain $s_{136}^0 = 39_{-17}^{+41} \text{ kpc}$ for $\alpha=1$ and $s_{136}^0 = 25_{-10}^{+25} \text{ kpc}$ for $\alpha=2$. Similarly to previous studies of cluster galaxies we report a strong truncation of galaxy halos in dense cluster environments compared to galaxy halos in the field.

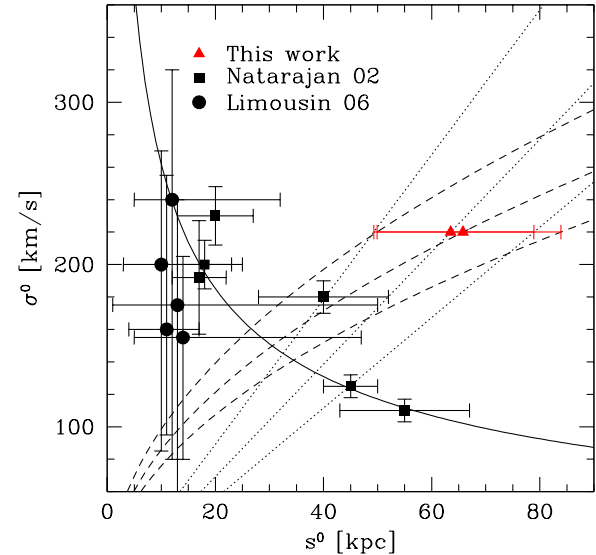


Fig. 3.— A comparison of three studies of galaxy truncation in the dense cluster environments. The red triangles are from this work, squares from Natarajan et al. (2002) and the circles from Limousin et al. (2006). The error bars shown are all $1-\sigma$. The dotted lines show the scaling of the best fit values and errors for $\alpha = 1$, the dashed lines for $\alpha = 2$. With the solid line we show the $s - \sigma$ pairs for a galaxy with a total mass of $5 \times 10^{11} M_\odot$.

7. Summary and Conclusions

In this paper we report the determination of the sizes of galaxy dark matter halos in galaxy cluster A1689. The strong lensing models for the cluster are constrained by 107 multiple images and an arc in 32 image systems. The strong constraints from these images enable us to study not only the global mass profile of the clusters but also the ones of the cluster galaxies. Assuming well motivated scaling laws between the truncation radius of a galaxy halo and its central velocity dispersion (as obtained with the fundamental plane and Faber-Jackson relations) we can study the combined effect of the cluster galaxies on the multiple images and the ensemble properties of the galaxies. This is the first time the sizes of galaxy halos have been measured using strong lensing only.

For a scaling law of the form $s_{\text{gal}} = s^0 \times (\sigma_{\text{gal}} / \sigma^0)^\alpha$ we find $s^0 = 64_{-28}^{+67} \text{ kpc}$ for $\alpha = 1$ and $s^0 =$

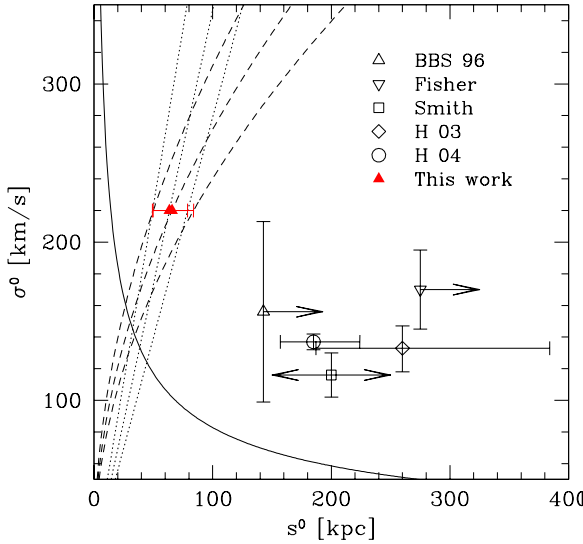


Fig. 4.— A comparison of studies of galaxy truncation in the field. The red triangles are from this work. The dotted lines show the scaling of the best fit values and errors for $\alpha = 1$, the dashed lines for $\alpha = 2$. The discrepancy is clear between the results obtained for galaxies in clusters and those in the field. Notice the difference in the horizontal scale between this figure and Fig. 3. The solid line shows the $s - \sigma$ pairs for a galaxy with a total mass of $5 \times 10^{11} M_{\odot}$.

66^{+72}_{-26} kpc for $\alpha = 2$. Both values are given for a fiducial galaxy velocity dispersion of $\sigma_0 = 220$ km/s. The errors are 2σ errors to show the clear asymmetry of the errors. The s^0 's are in good agreement with previously determined values in several other clusters using weak lensing (Natarajan et al. 1998, 2002; Limousin et al. 2006).

Galaxy halos in a cluster can be truncated either by the tidal field of the global cluster potential or harassment (Moore et al. 1996, 1998) by other cluster galaxies that strip the halos of galaxies in the central regions of cluster. Mergers of cluster galaxies on the other hand are extremely rare (Ghigna et al. 1998). Once the cluster has been formed the principal mechanism for truncation is the tidal stripping of galaxy halos by the global cluster potential (Ghigna et al. 2000). This is supported by the correlation between the density of the cluster at the core radius and the truncation radii of galaxies shown in Natarajan et al. (2002). The results presented here also support the tidal

stripping scenario.

This work was supported by the Deutsche Forschungsgemeinschaft, grant *SFB 375* “Astroteilchenphysik”. We would like to thank P. Schneider for giving us useful comments on the manuscript and M. Limousin for providing us with a draft of Limousin et al. (2006) and for interesting discussions.

Facilities: HST (ACS), HST (WFPC2).

REFERENCES

Balogh, M. L., Couch, W. J., Smail, I., Bower, R. G., & Glazebrook, K. 2002, MNRAS, 335, 10

Battaglia, G., Helmi, A., Morrison, H., Harding, P., Olszewski, E. W., Mateo, M., Freeman, K. C., Norris, J., & Shectman, S. A. 2005, MNRAS, 364, 433

Bender, R., Burstein, D., & Faber, S. M. 1992, ApJ, 399, 462

Bender, R., Saglia, R. P., & Gerhard, O. E. 1994, MNRAS, 269, 785

Brainerd, T. G. 2004, in AIP Conf. Proc. 743: The New Cosmology: Conference on Strings and Cosmology, ed. R. E. Allen, D. V. Nanopoulos, & C. N. Pope, 129–156

Brainerd, T. G., Blandford, R. D., & Smail, I. 1996, ApJ, 466, 623

Broadhurst, T., Benítez, N., Coe, D., Sharon, K., Zekser, K., White, R., Ford, H., Bouwens, R., Blakeslee, J., Clampin, M., Cross, N., Franx, M., Frye, B., Hartig, G., Illingworth, G., Infante, L., Menanteau, F., Meurer, G., Postman, M., Ardila, D. R., Bartko, F., Brown, R. A., Burrows, C. J., Cheng, E. S., Feldman, P. D., Golimowski, D. A., Goto, T., Gronwall, C., Herranz, D., Holden, B., Homeier, N., Krist, J. E., Lesser, M. P., Martel, A. R., Miley, G. K., Rosati, P., Sirianni, M., Sparks, W. B., Steinbring, S., Tran, H. D., Tsvetanov, Z. I., & Zheng, W. 2005, ApJ, 621, 53

dell'Antonio, I. P., & Tyson, J. A. 1996, ApJ, 473, L17+

Diego, J. M., Sandvik, H. B., Protopapas, P., Tegmark, M., Benítez, N., & Broadhurst, T. 2005, MNRAS, 362, 1247

Djorgovski, S., & Davis, M. 1987, ApJ, 313, 59

Dressler, A., Lynden-Bell, D., Burstein, D., Davies, R. L., Faber, S. M., Terlevich, R., & Wegner, G. 1987, ApJ, 313, 42

Duc, P.-A., Poggianti, B. M., Fadda, D., Elbaz, D., Flores, H., Chanial, P., Franceschini, A., Moorwood, A., & Cesarsky, C. 2002, A&A, 382, 60

Faber, S. M., & Jackson, R. E. 1976, ApJ, 204, 668

Fischer, P., McKay, T. A., Sheldon, E., Connolly, A., Stebbins, A., Frieman, J. A., Jain, B., Joffre, M., Johnston, D., Bernstein, G., Annis, J., Bahcall, N. A., Brinkmann, J., Carr, M. A., Csabai, I., Gunn, J. E., Hennessy, G. S., Hind-sley, R. B., Hull, C., Ivezić, Ž., Knapp, G. R., Limmongkol, S., Lupton, R. H., Munn, J. A., Nash, T., Newberg, H. J., Owen, R., Pier, J. R., Rockosi, C. M., Schneider, D. P., Smith, J. A., Stoughton, C., Szalay, A. S., Szokoly, G. P., Thakar, A. R., Vogeley, M. S., Waddell, P., Weinberg, D. H., York, D. G., & The SDSS Collaboration. 2000, AJ, 120, 1198

Gavazzi, R., Mellier, Y., Fort, B., Cuillandre, J.-C., & Dantel-Fort, M. 2004, A&A, 422, 407

Geiger, B., & Schneider, P. 1998, MNRAS, 295, 497

—. 1999, MNRAS, 302, 118

Ghigna, S., Moore, B., Governato, F., Lake, G., Quinn, T., & Stadel, J. 1998, MNRAS, 300, 146

—. 2000, ApJ, 544, 616

Halkola, A., Seitz, S., & M., P. 2006, Astro-ph, 0605470, accepted for publication in the MNRAS

Hartwick, F. D. A., & Sargent, W. L. W. 1978, ApJ, 221, 512

Hoekstra, H. 2003, MNRAS, 339, 1155

Hoekstra, H., Yee, H. K. C., & Gladders, M. D. 2004, ApJ, 606, 67

Hudson, M. J., Gwyn, S. D. J., Dahle, H., & Kaiser, N. 1998, ApJ, 503, 531

Limousin, M., Kneib, J. P., Bardeau, S., Natarajan, P., Czoske, O., Smail, I., Ebeling, H., & Smith, G. P. 2006, ArXiv Astrophysics e-prints

Limousin, M., Kneib, J.-P., & Natarajan, P. 2005, MNRAS, 356, 309

McKay, T. A., Sheldon, E. S., Racusin, J., Fischer, P., Seljak, U., Stebbins, A., Johnston, D., Frieman, J. A., Bahcall, N., Brinkmann, J., Csabai, I., Fukugita, M., Hennessy, G. S., Ivezić, Z., Lamb, D. Q., Loveday, J., Lupton, R. H., Munn, J. A., Nichol, R. C., Pier, J. R., & York, D. G. 2001, Astro-ph

Merritt, D. 1983, ApJ, 264, 24

Moore, B., Katz, N., Lake, G., Dressler, A., & Oemler, Jr., A. 1996, Nat, 379, 613

Moore, B., Lake, G., & Katz, N. 1998, ApJ, 495, 139

Natarajan, P., & Kneib, J.-P. 1997, MNRAS, 287, 833

Natarajan, P., Kneib, J.-P., & Smail, I. 2002, ApJ, 580, L11

Natarajan, P., Kneib, J.-P., Smail, I., & Ellis, R. S. 1998, ApJ, 499, 600

Prada, F., Vitvitska, M., Klypin, A., Holtzman, J. A., Schlegel, D. J., Grebel, E. K., Rix, H.-W., Brinkmann, J., McKay, T. A., & Csabai, I. 2003, ApJ, 598, 260

Smith, D. R., Bernstein, G. M., Fischer, P., & Jarvis, M. 2001, ApJ, 551, 643

Sofue, Y., & Rubin, V. 2001, ARA&A, 39, 137

Teague, P. F., Carter, D., & Gray, P. M. 1990, ApJS, 72, 715

Tormen, G., Diaferio, A., & Syer, D. 1998, MNRAS, 299, 728

Tyson, J. A., Valdes, F., Jarvis, J. F., & Mills, A. P. 1984, ApJ, 281, L59

Wilson, G., Kaiser, N., Luppino, G. A., & Cowie, L. L. 2001, ApJ, 555, 572

Zaritsky, D., Olszewski, E. W., Schommer, R. A., Peterson, R. C., & Aaronson, M. 1989, ApJ, 345, 759

Zekser, K. C., White, R. L., Broadhurst, T. J., Benítez, N., Ford, H. C., Illingworth, G. D., Blakeslee, J. P., Postman, M., Jee, M. J., & Coe, D. A. 2006, ApJ, 640, 639